Monte Carlo Simulations of Liquid Alkyl Ethers with the OPLS Potential Functions

James M. Briggs, Tooru Matsui, and William L. Jorgensen*

Department of Chemistry, Purdue University, West Lafayette, Indiana 47907

Received 17 January 1990; accepted 26 March 1990

Intermolecular potential functions have been developed for use in computer simulations of alkyl ethers. The simple OPLS model was adopted and parameterized to yield good descriptions of bimolecular and ion-molecule complexes as well as to reproduce experimental thermodynamic properties of liquid ethers. The principal testing featured Monte Carlo statistical mechanics simulations for liquid dimethyl ether (DME), ethyl methyl ether (EME), diethyl ether (DEE), and tetrahydrofuran (THF). Average errors of 1–3% are obtained for the computed densities and heats of vaporization including results for THF at pressures up to 5000 atm. The torsional motion about the central C—O bonds in EME and DEE was included in the simulations using rotational potential functions fit to results of molecular mechanics (MM2) calculations. The liquid-state environment is found to have negligible effect on the conformational equilibria.

INTRODUCTION

Monte Carlo and molecular dynamics simulations have been successfully applied to the study of organic and biochemical systems in solution.[1] A critical component of the calculations is the description of the intermolecular interactions. To this end, we have developed optimized potentials for liquid simulations (OPLS) primarily by fitting the results of many liquid and dilute solution Monte Carlo simulations directly to experimental condensed-phase data. Parameters have now been generated for water,[2] alkanes,[3] alcohols,[4] amides,[5] alkyl chlorides,[6] amines,[7] carboxylic esters and acids,[8] various sulfur[9] and nitrogen[10] compounds, and nitriles,[11] among others. A protein force field has been established[12] and the coverage has also been expanded to ions including ammonium,[13] carboxylate,[13] lithium,[14] sodium,[14] fluoride,[14] chloride,[14] *t*-butyl cation,[15] and several other organic ions.[7,16]

Since ethers are commonly used dipolar aprotic solvents, an effort is made here to update the previous TIPS parameters for alkyl ethers.[17–19] As representative cases, dimethyl ether (DME), ethyl methyl ether (EME), diethyl ether (DEE), and tetrahydrofuran (THF) have been studied. The standard OPLS philosophy is applied which is (1) to keep the form of the potentials simple and easy to evaluate, (2) to introduce as few new parameters as possible, and (3) to produce structural and thermodynamic properties in reasonable accord with experiment. In the previous studies of liquid alkyl ethers the simulations were carried out after the parameterization. In the current study, simulations were performed iteratively as part of the parameterization so better agreement with experiment is obtained. Furthermore, much structural and thermodynamic information is obtained from the simulations and is compared with experiment and previous theoretical work where possible. The details of the computations will be discussed next followed by the results for gas-phase complexes and the liquids.

COMPUTATIONAL DETAILS

Monte Carlo Simulations

Statistical mechanics simulations were carried out for the four pure alkyl ether liquids, DME, EME, DEE, and THF. Standard procedures such as Metropolis sampling, periodic boundary conditions and the isothermal-isobaric (NPT) ensemble were employed.[3–5,9] Each system consisted of 125 or 128 monomers in a cubic cell. Most of the simulations were run at 1 atm. DME was run at −24.6 °C,[20] its boiling point; EME was run at 25.0 °C and at its boiling point 7.35 °C;[20] DEE was run at 25.0 °C; THF was run at 25.0, 50.0, and finally 65.95 °C, its boiling point.[21] The boiling point of DEE is 34.55 °C.[20] In addition, THF was simulated at 30.0 °C and 1, 1054, 1566, 2095, 3000, 4000, 5000 atm.

Some of the other parameters for the simulation are given in Table I. The intermolecular interactions were spherically truncated at cutoff distances, r_c, based on the 0...0 separations. A

*To whom all correspondence should be addressed.

CCC 0192-8651/90/080958-14$04.00

Table I. Computational details of the Monte Carlo simulations for alkyl ether liquids.

Liquid	Number of configurations × 10^6		r_c, (Å)	Δr, (Å)	$\Delta\theta$, (deg)	$\Delta\Phi$, (deg)	ΔV, (Å^3)
	Equil	Averaging					
DME	0.2	1.5	11.0	0.25	25		400
EME	0.4	1.5	12.5	0.20	20	20	450
DEE	0.6	1.5	13.0	0.16	16	16	600
THF	0.4	1.5	12.5	0.20	20		450

correction was made for the Lennard–Jones interactions neglected beyond the cutoff. It amounts to ca. 4% of the total energy and was computed in a standard way.[3] New configurations were generated by randomly selecting a molecule, translating it in all three cartesian directions, rotating it about a chosen axis, and performing any appropriate internal rotations, one for EME and two for DEE. The ranges for distance, angle, dihedral angle and volume moves are $\pm\Delta r$, $\pm\Delta\theta$, $\pm\Delta\Phi$ and $\pm\Delta V$, respectively. They were chosen so that an acceptance rate for new configurations of ca. 40% was achieved. Volume moves were attempted every 600 configurations and involved scaling all of the intermolecular separations.

Each simulation consisted of equilibration and averaging phases. Initial configurations were taken from the earlier work[17,19] so that convergence of the energy and density needed only 0.2 to 0.6 M configurations. Statistical uncertainties ($\pm 1\sigma$) were calculated from the fluctuations in the averages over batches of 0.05 M configurations. The calculations were carried out on Sun 4, Silicon Graphics 4D, and Gould 32/8750 computers in our laboratory.

Intermolecular Potential Functions

The OPLS representation consists of Coulomb plus Lennard-Jones terms (eq. (1)). The interaction energy between two

$$\Delta E_{ab} = \sum_{i}^{\text{on } a} \sum_{j}^{\text{on } b} (q_i q_j e^2/r_{ij} + A_{ij}/r_{ij}^{12} - C_{ij}/r_{ij}^{6}) \quad (1)$$

molecules, a and b, is determined from the double sum over pairs of interacting sites on both a and b. Sites are positioned on the atomic nuclei and on carbon for methyl and methylene groups where a united atom representation is used. The combining rules for the Lennard–Jones parameters are $A_{ij} = (A_{ii}A_{jj})^{1/2}$ and $C_{ij} = (C_{ii}C_{jj})^{1/2}$. Furthermore, the A and C parameters can be written in terms of σ and ϵ where $A_{ii} = 4\epsilon_i\sigma_i^{12}$ and $C_{ii} = 4\epsilon_i\sigma_i^{6}$. Standard geometrical parameters were used as given in Table II.[22] All geometrical parameters except dihedral angles were held fixed throughout the simulations.

The initial charge and Lennard–Jones parameters were taken from earlier work on liquid ethers,[17] alkanes,[3] and sulfur compounds.[9] They were developed such that bimolecular and ion-molecule complexes are described well in the gas phase and finally so that the thermodynamic properties of the liquids are in reasonable accord with experiment. The introduction of new parameters was kept to a minimum. The final parameters are recorded in Table II. Standard alkyl group parameters[3] are used for groups that are at least one atom removed from the ether oxygen.

Table II. Geometrical and OPLS parameters for alkyl ethers.

Standard Geometrical Parameters[a]

O—C	1.41	∠COC	112.0	∠OCC	109.4[b]
CH_2—CH_2	1.53[b]	∠OCC	112.0		
CH_2—CH_3	1.516	∠COC	111.0[b]		

OPLS Parameters

atom or group	q, e	σ, Å	ϵ, kcal/mol
O (R_2O)	−0.50	3.000	0.170
CH_3 (CH_3OR)	0.25	3.800	0.170
CH_3 (CH_3ROR)	0.00	3.905	0.175
CH_2 (RCH_2OR)	0.25	3.800	0.118
CH_2 (—CH_2ROR—)[b]	0.00	3.905	0.118

[a]Bond lengths in angstroms, bond angles in degrees.
[b]Parameters for THF.

It was found in earlier studies of liquid *N*-alkyl amides[5] and sulfur compounds[9] that a σ of 3.80 Å and an ϵ of 0.170 kcal/mol were appropriate for methyl groups adjacent to nitrogen or sulfur, while a σ and ϵ of 3.80 and 0.118 were used for corresponding methylene groups. These parameters also work out well for alkyl ethers and were adopted here. The charge of −0.50 for the ether oxygen from the revised TIPS parameters[17] also proved appropriate. It yields a dipole moment of 1.89 D for DME as compared with an experimental moment of 1.30 D.[23] Often, a dipole moment from the partial charges that is ca. 15–25% greater than experiment is needed to obtain reasonable interaction energies and liquid thermodyanmics.[5,9,17] The σ and ϵ for alcohol oxygens are 3.07 and 0.17,[4] respectively, whereas those for ether oxygens from the revised TIPS parameters are 3.07 and 0.18.[17] It was found here that a slightly smaller σ, 3.00, and an ϵ of 0.17 give better results.

Internal Rotation

Although bond lengths and angles are fixed throughout the simulations, dihedral angles are not. For EME and DEE, rotations were allowed about the central C—O bonds.[17,24] The form of the torsional potential for EME, which has only one dihedral angle, is given by the Fourier expansion in eq. (2). For molecules that have two dihedral angles, like DEE, the

$$V(\Phi) = 1/2V_1(1 + \cos \Phi) + 1/2V_2(1 - \cos 2\Phi) + 1/2V_3(1 + \cos 3\Phi) \quad (2)$$

Fourier series needs to be augmented by a 1–5 Lennard–Jones potential as shown in eq. (3).

$$V(\Phi_1, \Phi_2, r_{15}) = V(\Phi_1) + V(\Phi_2) + 4\epsilon[(\sigma/r_{15})^{12} - (\sigma/r_{15})^6] \quad (3)$$

As in previous studies of alkanes,[3] alcohols,[4] and sulfur compounds[9] the coefficients were obtained from a fit to results of MM2 calculations.[25–27] For both EME and DEE, a good fit was obtained with $V_1 = 2.8827$, $V_2 = -0.6507$, and $V_3 = 2.2183$ kcal/mol, and with Lennard–Jones parameters, $\sigma = 2.745$ Å and $\epsilon = 0.008$ kcal/mol, for eq. (3).

A plot of the rotational energy function for EME appears at the top of Figure 1. EME has one trans and two mirror image gauche forms. From MM2 results the trans form is 1.54 kcal/mol lower in energy than gauche. The *t* to *g*, *g* to *t*, and g^+ to g^- barrier heights are 2.45, 0.90, and 3.55 kcal/mol, respectively. The present torsional potential gives a gauche-trans energy difference of 1.51 kcal/mol and *t* to *g*, *g* to *t*, and g^+ to g^- barrier heights of 2.48, 0.97, and 3.59 kcal/mol. Experimental values for these

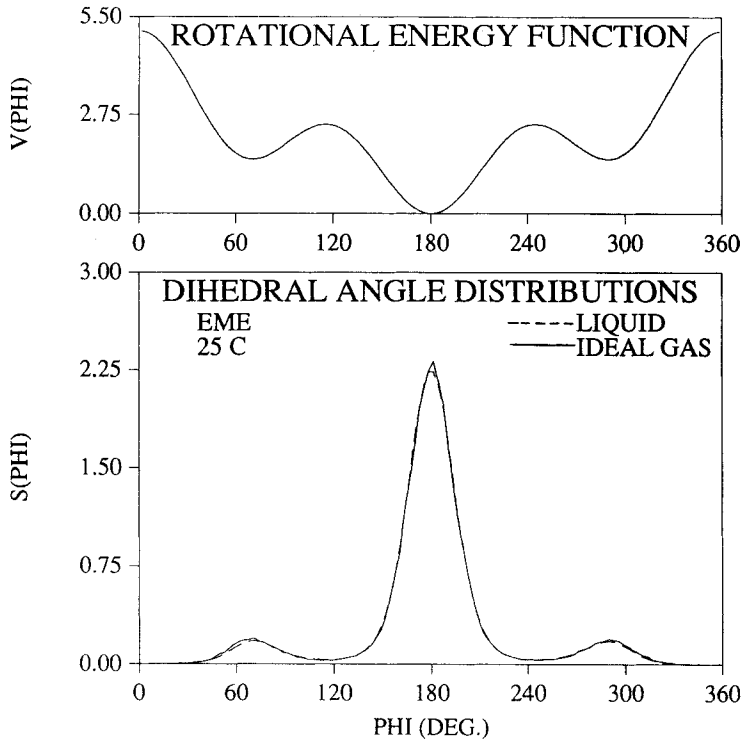

Figure 1. Rotational energy function and dihedral angle distributions for EME. Units are kcal/mol for $V(\Phi)$ and mole percent per degree for $S(\Phi)$ in Figures 1, 2.

barriers from IR and Raman studies are 2.93, 1.80, and 2.96 kcal/mol.[28] This implies a gauche-trans energy difference of 1.13 kcal/mol. However, a gauche-trans energy difference of 1.5 ± 0.2 kcal/mol has been reported from an electron diffraction study.[29] The latter work also gave a dihedral angle for the gauche form of 84 ± 6°. In a previous study of EME,[17] *ab initio* molecular orbital calculations were performed with the STO-3G and 4-31G basis sets. These calculations yielded a dihedral angle of 85° for the gauche conformer, a gauche-trans energy difference of 1.96 kcal/mol and *t* to *g*, *g* to *t*, and g^+ to g^- barrier heights of 2.33, 0.37, and 4.92 kcal/mol. A dihedral angle of 72° is found by MM2 and one of 71° results from the present torsional potential.

DEE has four possible conformational minima, trans-gauche (*tg*), two gauche-gauche (*gg*), and trans-trans (*tt*). The MM2 results place g^+g^+ 3.2 kcal/mol above *tt*, and *tg* 1.6 kcal/mol above *tt*. The g^+g^- form is not found to be a minimum and is about 8 kcal/mol above *tt*. For comparison, an IR experiment[30a] put *tg* 1.4 kcal/mol above *tt* and a Raman investigation gave a difference of 1.15 ± 0.11 kcal/mol.[30b] The present rotational potential gives g^+g^+ 3.1 kcal/mol above *tt*, and *tg* 1.5 kcal/mol above *tt*. In a previous study of THF, it was concluded that inclusion of pseudorotation to account for puckering of the ring had negligible effect on the liquid thermodynamics and radial distribution functions.[19] Therefore the ring was held planar in the present work.

RESULTS AND DISCUSSION

Bimolecular and Ion-Molecule Complexes

Geometry optimizations using the OPLS potentials have been carried out for several complexes of DME, the results of which are summarized in Table III. The forms of the complexes are shown below:

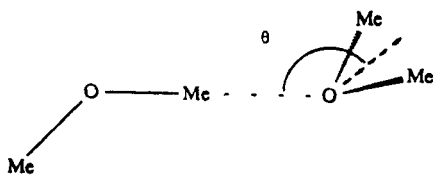

linear

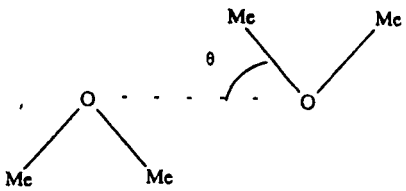

cyclic

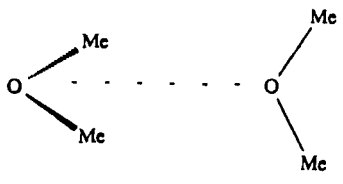

bifurcated

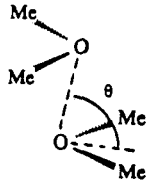

antiparallel

The monomer geometries were held fixed while the distance 00 (r) and the angle (θ) were optimized. The present results for DME are in accord with previous studies.[17,18] The relative ordering for the interaction energies is the same, namely: bifurcated < antiparallel < linear < cyclic. The energy of the linear TIP4P water-DME complex for the present study is −5.77 kcal/mol which is in good accord with a previous *ab initio* estimate with the 6-31G(d) basis set of −5.73 kcal/mol.[31a] The revised TIPS value is −4.79 kcal/mol.[17]

A final check of the parameters was done by computing the interaction energies of the lithium and sodium ion-molecule complexes for DME. Previously reported parameters for lithium and sodium[14] were used and yield interaction energies of −31.6 and −22.6 kcal/mol, respectively. These results are similar to those with the revised TIPS parameters, which are −30.9 and −22.1 kcal/mol. *Ab initio* estimates to these energies have been made at both the 3-21G//3-21G and 6-31G(d)//3-21G levels.[31b] The lithium and sodium-DME interaction energies at the latter level are −41.2 and −28.2 kcal/mol, respectively. The experimental lithium affinity for DME is −39.5 kcal/mol.[31c] It should be noted that the results from such *ab initio* calculations, uncorrected for vibrational effects, typically overestimate the ion affinities by ca. 4 kcal/mol.[31b] Attempts to improve the predicted ion-molecule interaction energies should probably focus on explicit treatment of polarization; adjustments in the present format are accompanied by poorer bimolecular interaction energies and worse descriptions of the liquids.

Liquid Thermodynamics

The calculated physical and thermodynamic results for the four liquid ethers are given in Tables IV–VI. The heat of vaporization at 1 atm is calculated from the relationship given in eq. 4.

$$\Delta H_{vap} = E_{intra}(g) - (E_i(1) + E_{intra}(1)) + RT \quad (4)$$

Table III. Calculated complexation energies (kcal/mol) and geometrical parameters.

Complex	xy	r_{xy}, Å	ABC[a]	θABC, (deg)	$-\Delta E$[b]
Linear $(CH_3OCH_3)_2$	OO	4.83	OOb	149	1.57
Cyclic $(CH_3OCH_3)_2$	OO	4.22	OOC	62	1.37
Bifurcated $(CH_3OCH_3)_2$	OO	4.08			2.21
Antiparallel $(CH_3OCH_3)_2$	OO	3.96	OOb	78	1.73
$HOH\ldots O(CH_3)_2$	HO	2.75	OOb	155	5.77
$Li^+\ldots O(CH_3)_2$	LiO	1.84	LiOC	124	31.57
$Na^+\ldots O(CH_3)_2$	NaO	2.21	NaOC	124	22.55

[a] b is the bisector of the CH_3OCH_3 angle.
[b] $-\Delta E$ is the dissociation energy for the complex, $M\ldots N \rightarrow M + N$.

Table IV. Energetic results (kcal/mol) for liquid alkyl ethers.

Liquid	T, °C	$-E_i$	E_{intra}(g)	E_{intra}(l)	ΔH_{vap} Calcd	ΔH_{vap} Exptl
DME	−24.8	4.52 ± 0.01	0.0	0.0	5.01 ± 0.01	5.14[a]
EME	7.35	5.44 ± 0.01	0.523	0.519 ± 0.010	5.97 ± 0.01	5.91[b]
	25.0	5.23 ± 0.02	0.573	0.581 ± 0.008	5.82 ± 0.02	5.6[b]
DEE	25.0	6.53 ± 0.02	1.144	1.232 ± 0.009	7.04 ± 0.02	6.56[b]
THF	25.0	6.95 ± 0.02	0.0	0.0	7.54 ± 0.02	7.61[c]
	50.0	6.67 ± 0.02	0.0	0.0	7.31 ± 0.02	7.33[d]
	65.95	6.50 ± 0.02	0.0	0.0	7.17 ± 0.02	7.13[e]

[a] Reference 32.
[b] Reference 20.
[c] Reference 33.
[d] Interpolated from data given in Reference 39.
[e] Reference 39.

Table V. Molecular volumes and densities for liquid alkyl ethers.

Liquid	T, °C	V, Å^3 Calcd	V, Å^3 Exptl	d, g/cm^3 Calcd	d, g/cm^3 Exptl
DME	−24.8	106.9 ± 0.3	104.1[a]	0.715 ± 0.002	0.7345[a]
EME	7.35	140.0 ± 0.5	138.5[b]	0.712 ± 0.003	0.7205[b]
	25.0	143.8 ± 0.4	144.1[c]	0.693 ± 0.002	0.6922[c]
DEE	25.0	169.5 ± 0.3	173.9[c]	0.725 ± 0.001	0.7076[c]
THF	25.0	135.7 ± 0.2	136.0[d]	0.882 ± 0.001	0.884[d]
	50.0	139.5 ± 0.2	139.4[e]	0.858 ± 0.001	0.859[e]
	65.95	142.3 ± 0.3		0.841 ± 0.002	

[a] Reference 34.
[b] Reference 35.
[c] Reference 20.
[d] Reference 33.
[e] Reference 40.

$E_{intra}(g)$ is the internal rotational energy in the gas phase which is calculated from Boltzmann distributions for eqs. (2) and (3). $E_i(1)$ is the total intermolecular energy for the liquid, $E_{intra}(1)$ is the torsional energy in the liquid phase and RT corrects for expansion to the gas. The constant pressure liquid heat capacity, $C_p(1)$, is calculated from fluctuations in the total intermolecular energy, E_i, plus the ideal gas heat capacity, C_p°, less R. The isothermal compressibility, κ, is calculated from fluctuations in the volume, while the isobaric expansivity, α, is calculated from fluctuations in the enthalpy and volume. The latter two quantities are very slow in converging and have large statistical uncertainties.[36]

The computed heats of vaporization are compared with experimental values in Table IV. All of these values are in reasonable accord with experiment deviating by an average of 3%. The same trend of increasing ΔH_{vap} with increasing

Table VI. Heat capacities (cal/mol-deg)) and isothermal compressibilities (atm^{-1}) for liquid alkyl ethers.

Liquid	T, °C	$C_P°$ (g)	$C_p(1)$ Calcd	$C_p(1)$ Exptl	$10^6\kappa$, Calcd
DME	−24.8	15.4[a]	26.0 ± 1.2	24.7[b]	179 ± 17
EME	7.35	21.8[a]	33.1 ± 1.1		175 ± 20
	25.0	21.8[a]	33.5 ± 1.1		190 ± 21
DEE	25.0	28.0[a]	41.0 ± 1.3	41.36[a]	114 ± 12
THF	25.0	18.1[c]	26.6 ± 1.0	29.56[d]	78 ± 6

[a]Reference 20.
[b]Reference 32.
[c]Reference 34.
[d]Reference 35.

length of the molecule for the acyclic series is reproduced by the OPLS potentials and is primarily attributable to increasing Lennard–Jones attraction. The heat of vaporization of THF is notably higher than for DEE; THF is more compact (Table V) and can accommodate greater surface-surface contact.

The calculated volumes and densities (Table V) also agree well with experiment deviating only by an average of 1%. The volume of a THF molecule is seen to be nearly 40 Å^3 less than for DEE, i.e., a greater difference than the methylene group increment for the acyclic series. The computed heat capacities, given in Table VI, are also in accord with experiment. It should be noted, however, that the ideal gas C_p° less R makes a substantial contribution to $C_p(1)$ and that this property, along with κ and α, converges more slowly than the total energy or volume.[37] Nevertheless, the calculated expansivities are not unreasonable. For DME, EME at 25 °C, DEE and THF, the computed α's are 205 ± 22, 162 ± 20, 112 ± 14, and 96 ± 10 × 10^{-5} deg^{-1}, while the experimental values are 187[34], 171[35], 160[27], and 110[38] × 10^{-5} deg^{-1}, respectively. Overall, the OPLS parameters give a good description of the physical and thermodynamic properties of the liquid ethers. The deviations from experiment encountered here are similar to those obtained from previous studies of liquid hydrocarbons,[3] amides,[5] alcohols,[4] and sulfur compounds.[9]

The results from the THF simulations at 30 °C and elevated pressures can be found in Table VII. Each simulation consisted of an equilibration phase of 2 M configurations and an averaging phase of 4 M. Since the pressure differences between runs were quite large, these simulations were equilibrated and averaged about twice as long as the other simulations to insure precise results. The computed densities are in remarkable accord with experimental data (within 1%). Previously, pure liquid Monte Carlo simulations of methanol,[42a] n-butane,[42b] and 1,2-dichloropropane[42c] at high pressure produced densities that were within 3% of the experimental values. These results provide further evidence of the robustness of the potential functions under a variety of conditions.

Conformational Equilibria

The conformer populations for EME and DEE are given in Table VIII for the gas and liquid states. It can be seen that the condensed phase has an insignificant effect on the conformational equilibria of these simple ethers. The same is

Table VII. Computed densities and intermolecular energies for THF at elevated pressures and 30 °C.

P, atm	d, g/cm^3 Calcd.	d, g/cm^3 Exptl.[a]	$-E_i$ kcal/mol calcd.
1	0.8797 ± 0.0011	0.8730 ± 0.0001	6.91 ± 0.01
1054	0.9455 ± 0.0008	0.9345 ± 0.0001	7.39 ± 0.01
1566	0.9691 ± 0.0008	0.9592 ± 0.0001	7.55 ± 0.01
2095	0.9839 ± 0.0006	0.9814 ± 0.0001	7.62 ± 0.01
3000	1.0139 ± 0.0007	1.0126 ± 0.0001[b]	7.78 ± 0.01
4000	1.0405 ± 0.0005	1.0376 ± 0.0001[c]	7.90 ± 0.01
5000	1.0604 ± 0.0006	1.0632 ± 0.0001[d]	7.95 ± 0.01

[a]Reference 41.
[b]Density at 2965 atm.
[c]Density at 3995 atm.
[d]Density at 5057 atm.

Table VIII. Calculated conformer populations.

Compound	T, °C	Conformer	Gas (%)[a]	Liquid (%)[b]
EME	7.35	t	87.1	86.9 ± 0.5
		g	12.9	13.1 ± 0.5
	25.0	t	85.2	84.3 ± 0.5
		g	14.8	15.7 ± 0.5
DEE	25.0	tt	72.5	70.3 ± 1.0
		tg	25.3	26.4 ± 1.0
		g^+g^+	1.1	1.3 ± 0.2
		g^+g^-	1.1	2.0 ± 0.2

[a]Calculated from a Boltzmann distribution.
[b]Results from the Monte Carlo simulations.

true for the hydrocarbons[3] and sulfur compounds[9] previously studied. It should be noted that in the OPLS functions, the dipole moments for the ethers do not change with changes in the dihedral angles since the β atoms are neutral. The same is true for the OPLS description of sulfides and thiols.[9] Plots of the dihedral angle distributions for EME and DEE are given in Figures 1 and 2. It is again apparent that the conformational populations are not affected upon going from the gas to the liquid state. Thorough sampling of the conformation spaces was attained which is reflected in the symmetry and smoothness of the distributions.

Radial Distribution Functions

Some of the computed radial distribution functions (rdfs) for the liquid alkyl ethers are given in Figures 3–7. $g_{xy}(r)$ represents the probability of finding atoms of type y at a distance r from atom x normalized for the bulk density of y atoms. In Figures 4 and 5, CO corresponds to a carbon atom alpha to oxygen. In Figure 6, Cl refers to a carbon beta to oxygen. Overall the computed rdfs are very similar to those from the earlier work and will not be discussed in detail.[17,19] All of the ethers studied exhibit a maximum in g_{OO} at about 3.8 Å. The first minima in g_{OO} for DME, EME, DEE, and THF are at 7.1, 7.5, 7.9, and 7.7 Å, respectively. Integration out to these minima yields 13.2, 11.8, 11.4, and 13.2 neighbors for DME, EME, DEE, and THF.

One of the more interesting features of these rdfs is the shoulder at ca. 3.8 Å in the g_{OC} rdfs (Fig. 4). This indicates that some of the neighbors exhibit some more special interactions with one another. In accord with the previous study it was determined upon integration out to 4 Å that, on the average, four favorable OC and CO interactions were present for DME.[17] Based upon that result a pseudo water-like structure could be imagined. However, it does not stand out in stereoplots such as Figure 8. The stereoplot of the final configuration of DME, as shown in Figure 8, also confirms the lack of obvious organization in the liquid. The periodicity of the cell should be remembered when viewing the cube; molecules that are near a face of the cell are also near molecules on the opposite face. Several favorable OC interactions can be seen like the bifurcated dimer in the lower left corner of

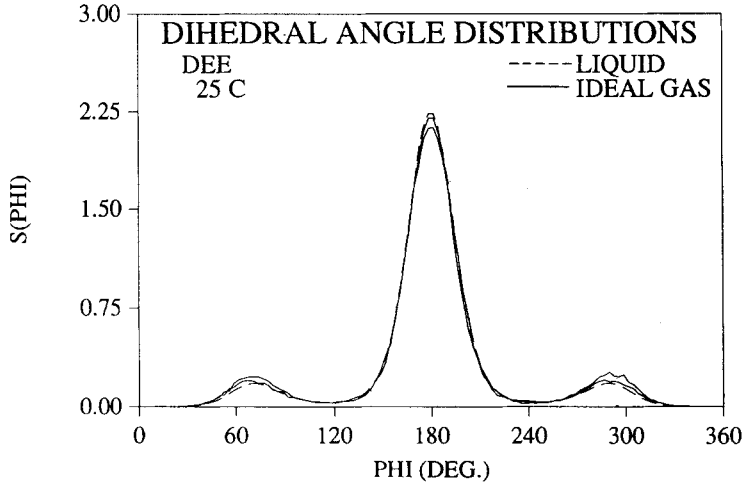

Figure 2. Dihedral angle distributions for DEE. Separate curves are shown for the two dihedral angles for DEE in the liquid.

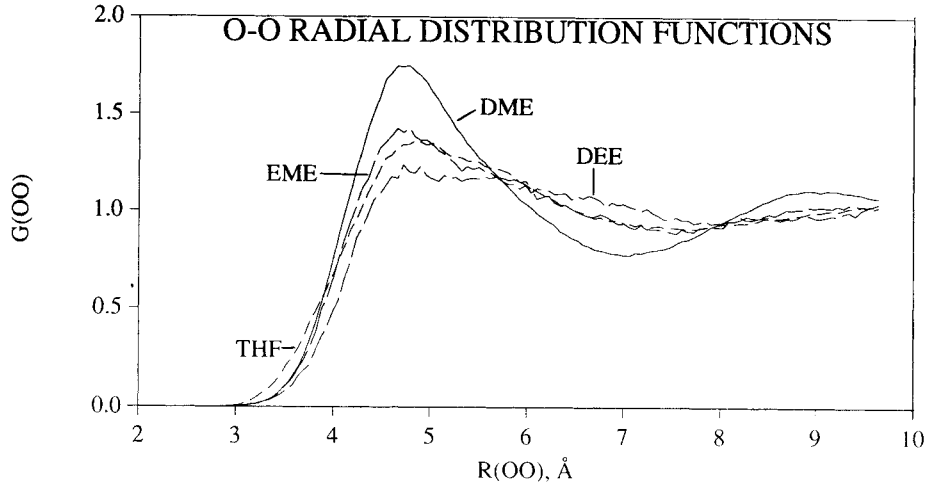

Figure 3. O—O radial distribution functions for DME, EME, DEE, and THF. Distances are in angstroms throughout.

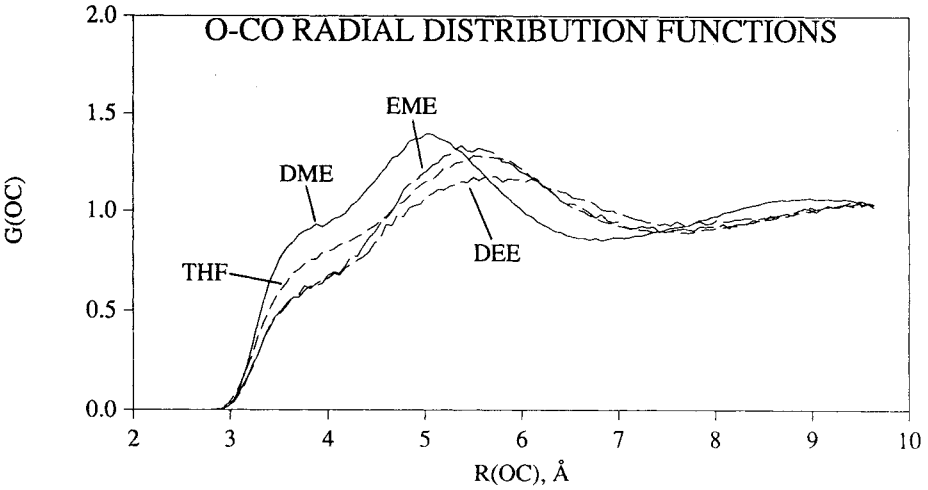

Figure 4. O—C_O radial distribution functions for DME, EME, DEE and THF. C_O is a carbon alpha to the ether oxygen.

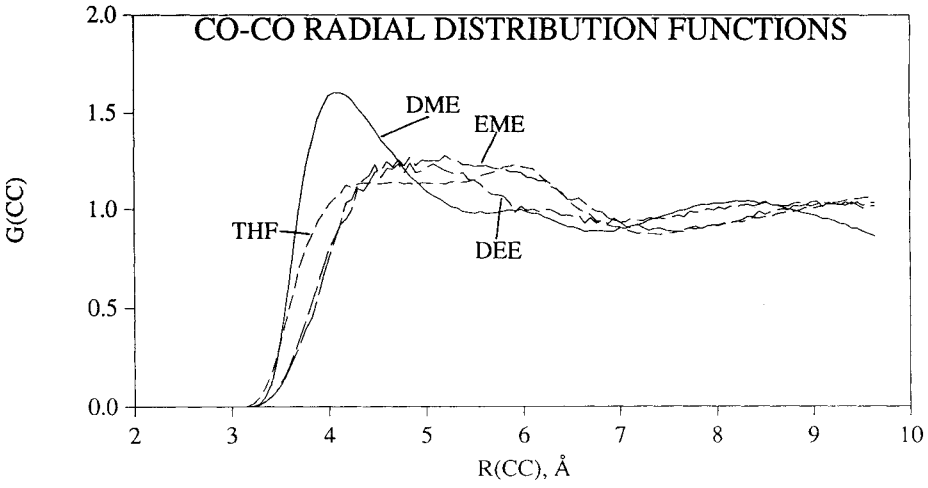

Figure 5. C_O—C_O radial distribution functions for DME, EME, DEE, and THF.

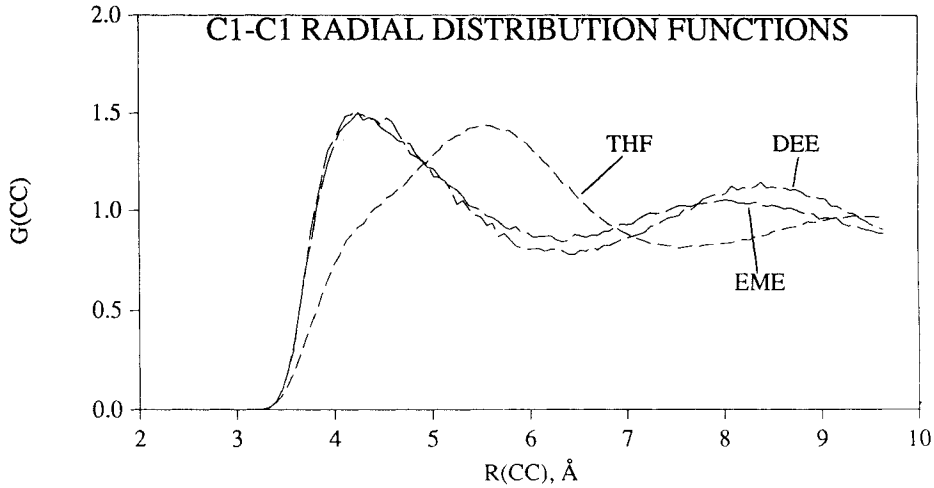

Figure 6. C_1—C_1 radial distribution functions for EME, DEE and THF. C_1 is a carbon beta to the ether oxygen.

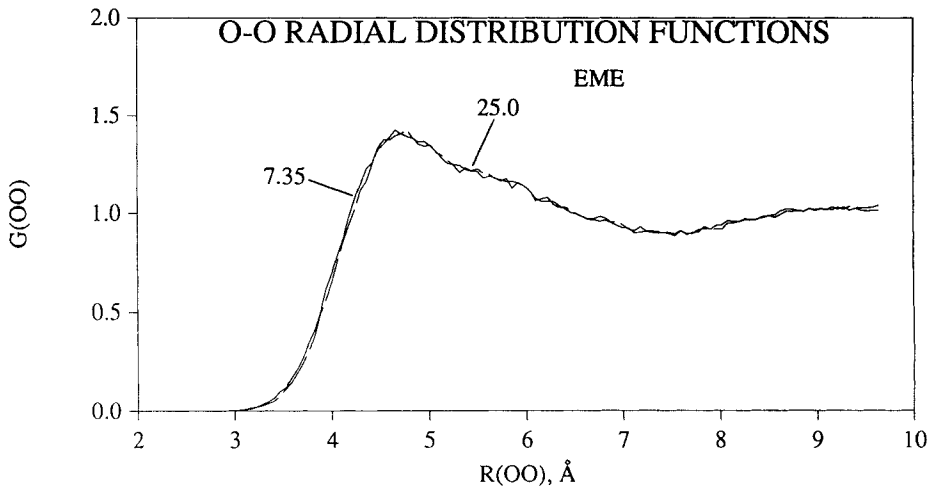

Figure 7. O—O radial distribution functions for EME at 7.35 °C and 25 °C.

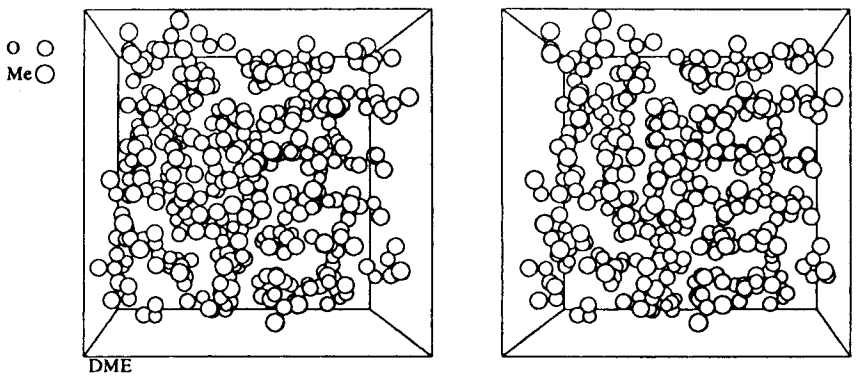

Figure 8. Stereoplot of the last configuration from the Monte Carlo simulation of DME run at −24.8 °C.

Figure 8. On the other hand, many less favorable CC contacts can be seen which disorders the liquid as compared to liquid water.

The other acyclic ethers, EME and DEE, are even less ordered than DME, as indicated by the reduced peak amplitudes in the rdfs. Stereoplots of the other three liquid ethers are in Figures 9–11. It should be noted that the increase in disorder is in part due to the increase in temperature by ca. 50 °C from DME to EME. In accord with the computed populations given in Table VIII, very few gauche bonds are present. As mentioned earlier two simulations were run for EME, one at 7.35 °C, its boiling point, and one at 25 °C. It is clear from Figure 7 that an 18 °C differential has very little effect on the rdfs. All rdfs at the two temperatures are essentially identical. The same is true for all of the rdfs for THF at the three temperatures studied (25.0, 50.0, and 65.95 °C).

THF shows more short O...CH_2 contacts than DEE which, in part, can be explained by the lesser number of degrees of freedom, both because of the ring constraint and the requirement for planarity of the ring. Some Coulombically favorable OC and CO interactions can be obtained by the following types of arrangements:

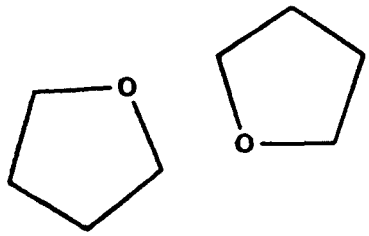

side to side

face to face

Several of these can be seen in the liquid in Figure 11.

The g_{OO} rdfs for THF at 30.0 °C and elevated pressures are found in Figure 12. As expected,[42] there is some sharpening of structure with increasing pressure accompanied by an inward shift of the first peak in the rdf. In view of the 17% compression of the liquid in going from 1 to 5000 atm, the effects on the liquid structure are notably modest.

Energy Distributions

During the simulations the energetic environments of the molecules were monitored. The total intermolecular bonding energy distributions for monomers (Fig. 13) display the same basic features as in a previous study.[17,19] As the length of the acyclic molecule increases, the average total bonding energy shifts to lower energy. This is due to the increase in van der Waals' attractions. As the temperature of the liquid decreases for EME the bonding energy distribution also shifts slightly to lower energy and narrows as seen in Figure 14. Similarly, the distribution is narrower for DME in Figure 13 owing to the lower temperature for that simulation. The ranges for the larger molecules are also expected to be broadened some because they have a greater variety of interactions with their neighbors, as noted earlier.[3,17] The bonding energy distribution for THF is shifted slightly to lower energy and is narrower than that for DEE. This is consistent with the higher density and the more favorable interactions reflected in the radial distribution functions for THF.

Energy pair distributions represent the distribution of individual molecule-molecule interaction energies. The spikes at 0 kcal/mol in Figure 15 reflect the interactions with the many distant molecules in the bulk. Energy pair distributions for nonpolar liquids are unimodal whereas those for strongly polar organic liquids (μ > ca. 2 D) are bimodal.[11] The distributions for the ethers are somewhere in between, being weakly bimodal. The strongest pair interaction energy for DME is ca. −2.1 kcal/mol which is in accord with the optimal pair interaction energy for the bifurcated dimer in Table III. Integration of the shoulder for DME to −0.9 kcal/mol leads to ca. four neighbors consistent with the number of short O...C contacts. Integration to −1.3 and −1.2 kcal/mol leads to ca. three and four neighbors for DEE and THF, respectively. EME has no distinct shoulder, in accord with the previous study.[17] The dimer interactions begin at −3.0, −3.6, and −3.2 kcal/mol for EME, DEE, and THF. The modest interaction energies and weak bimodal character in the energy pair distributions are consistent with the general picture of limited structure for the liquid ethers.

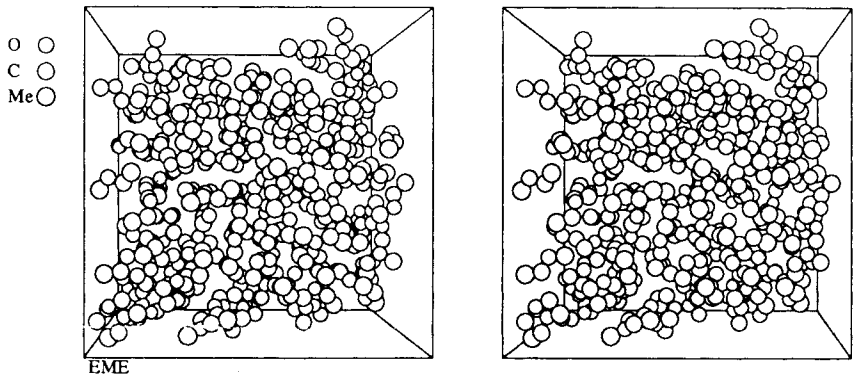

Figure 9. Stereoplot of the last configuration from the Monte Carlo simulation of EME run at 25 °C.

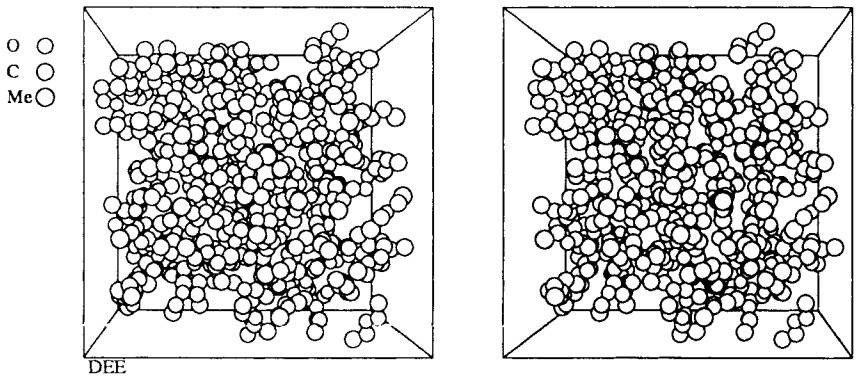

Figure 10. Stereoplot of the last configuration from the Monte Carlo simulation of DEE run at 25 °C.

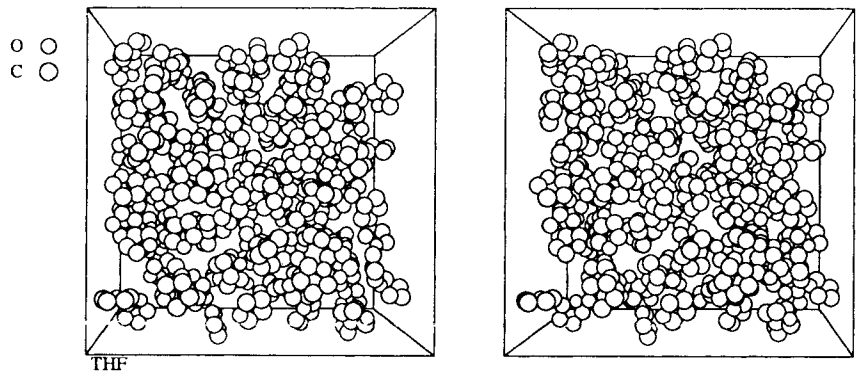

Figure 11. Stereoplot of the last configuration from the Monte Carlo simulation of THF run at 25 °C.

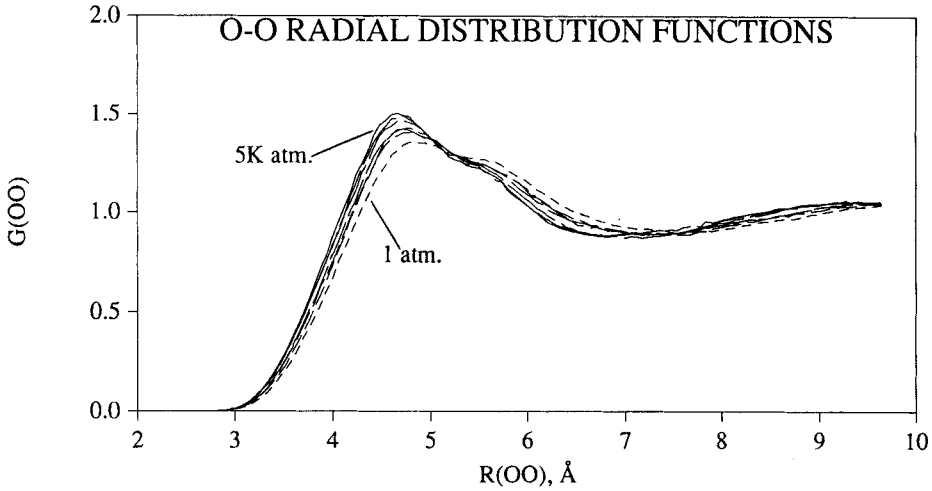

Figure 12. O—O radial distribution functions for THF at 30 °C and 5000 (solid line), 4000, 3000, 2095, 1566, 1054, and 1.0 atm (smallest dashed line). The intervening pressures are represented by dashed lines with intermediate length dashes.

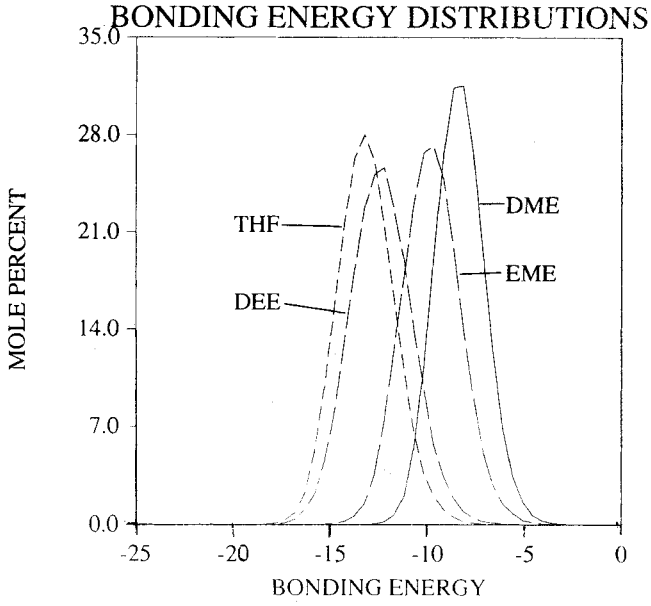

Figure 13. Distributions of the individual interaction energies (kcal/mol) between molecules in liquid DME, EME (25 °C), DEE and THF. Units for the ordinate and mole percent per kcal/mol.

CONCLUSION

Improved potential functions have been provided for liquid alkyl ethers that are suitable for use in simulations of ethereal solutions. The functions have been tested on gas-phase complexes and the thermodynamic and physical properties of the liquids. The average errors in densities and heats of vaporization are 1–3%. The present results also recomfirmed the lack of condensed phase effects on the conformational equilibria for ethers and the limited liquid structure characteristic of weakly polar organic fluids.

Gratitude is expressed to the National Institute of Health and the National Science Foundation for support.

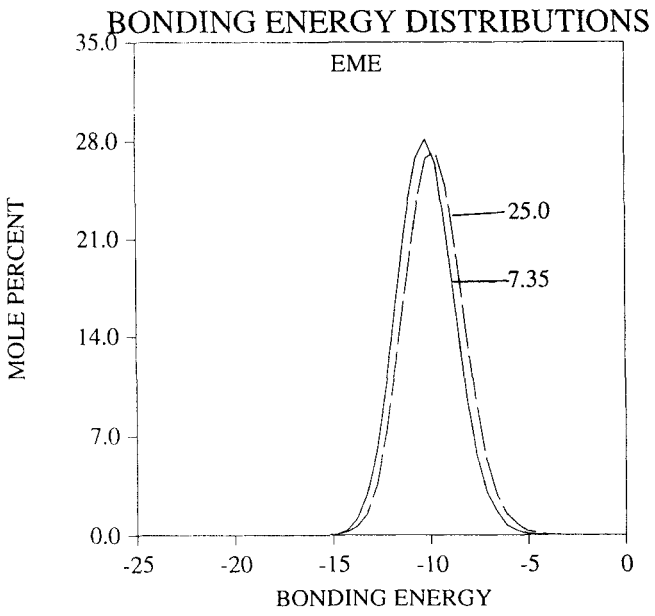

Figure 14. Distributions of the total intermolecular bonding energies for EME at 7.35 °C and 25 °C. Units as in Figure 12.

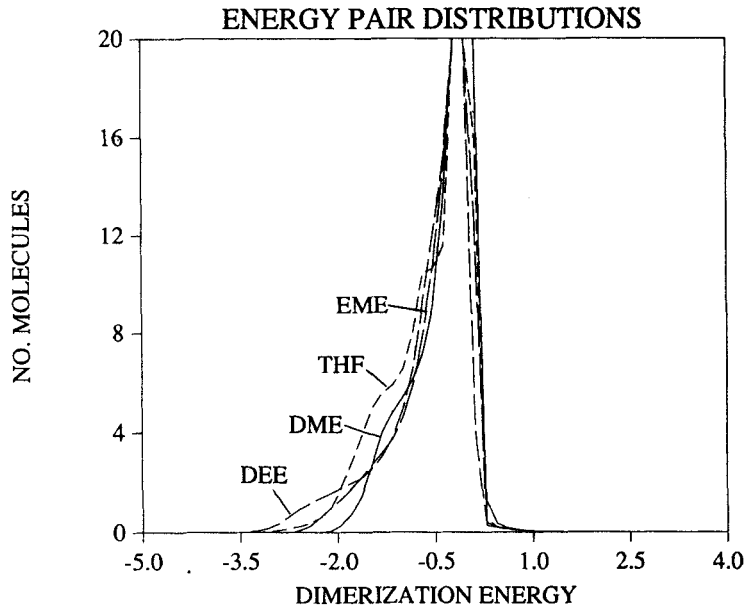

Figure 15. Distributions of the individual interaction energies (kcal/mol) between molecules in liquid DME, EME (25 °C), DEE and THF. Units for the ordinate are number of molecules per kcal/mol.

References

1. D. L. Beveridge and W. L. Jorgensen, Eds., *Computer Simulation of Chemical and Biomolecular Systems, Ann. N.Y. Acad. Sci.*, **482** (1986).
2. W. L. Jorgensen, J. Chandrasekhar, J. D. Madura, R. W. Impey, and M. L. Klein, *J. Chem. Phys.*, **79,** 926 (1983). W.L. Jorgensen and J. D. Madura, *Mol. Phys.*, **56,** 1381 (1985).
3. W. L. Jorgensen, J. D. Madura, and C. J. Swenson, *J. Am. Chem. Soc.*, **106,** 6638 (1984).
4. W. L. Jorgensen, *J. Phys. Chem.*, **90,** 1276 (1986).
5. W. L. Jorgensen and C. J. Swenson, *J. Am. Chem. Soc.*, **107,** 569 (1985).
6. W. L. Jorgensen, *J. Phys. Chem.*, **87,** 5304 (1983). W. L. Jorgensen and B. Bigot, *J. Phys. Chem.*, **86,** 2867 (1982).
7. W. L. Jorgensen and J. M. Briggs, *J. Am. Chem. Soc.*, **111,** 4190 (1989).
8. J. M. Briggs, T. B. Nguyen, and W. L. Jorgensen, submitted for publication.
9. W. L. Jorgensen, *J. Phys. Chem.*, **90,** 6379 (1986).
10. W. L. Jorgensen, J. M. Briggs, and L. M. Contreras, *J. Phys. Chem.*, **94,** 1683 (1990).
11. W. L. Jorgensen and J. M. Briggs, *Mol. Phys.*, **63,** 547 (1988).
12. W. L. Jorgensen and J. Tirado-Rives, *J. Am. Chem. Soc.*, **110,** 1657 (1988).

13. W. L. Jorgensen and J. Gao, *J. Phys. Chem.*, **90,** 2174 (1986).
14. J. Chrandrasekhar, D. C. Spellmeyer, and W. L. Jorgensen, *J. Am. Chem. Soc.*, **106,** 903 (1984).
15. W. L. Jorgensen, J. K. Buckner, S. E. Huston, and P. J. Rossky, *J. Am. Chem. Soc.*, **109,** 1891 (1987).
16. W. L. Jorgensen, J. M. Briggs, and J. Gao, *J. Am. Chem. Soc.*, **109,** 6857 (1987).
17. W. L. Jorgensen and M. Ibrahim, *J. Am. Chem. Soc.*, **103,** 3976 (1981).
18. W. L. Jorgensen, *J. Am. Chem. Soc.*, **103,** 335 (1981).
19. J. Chandrasekhar and W. L. Jorgensen, *J. Chem. Phys.*, **77,** 5073 (1982).
20. D. D. Wagman, W. H. Evans, V. B. Parker, R. H. Schumm, I. Halow, S. V. Bailey, K. L. Churney, and R. L. Nuttall, *J. Phys. Chem. Ref. Data. Suppl. 2,* **11,** 1 (1982).
21. J. A. Riddick and W. B. Bunger, *Organic Solvents,* Wiley-Interscience, New York, 1970, 3rd ed.
22. M. D. Harmony, V. W. Laurie, R. L. Kuczkowski, R. H. Schwendeman, D. A. Ramsay, F. J. Lovas, W. J. Lafferty, and A. G. Maki, *J. Phys. Chem. Ref. Data Ser.*, **8,** 619 (1979).
23. R. J. Abraham and B. Hudson, *J. Comp. Chem.*, **5,** 562 (1984).
24. W. L. Jorgensen, *J. Phys. Chem.*, **87,** 5304 (1983).
25. N. L. Allinger and D. Y. Chung, *J. Am. Chem. Soc.*, **98,** 6798 (1976).
26. U. Burkert, *Tetrahedron,* **35,** 1945 (1979).
27. N. L. Allinger and S. H.-M. Chang, *Tetrahedron,* **33,** 1561 (1977).
28. J. R. Durig and D. A. C. Compton, *J. Chem. Phys.*, **69,** 4713 (1978).
29. K. Oyanagi and K. Kuchitsu, *Bull Chem. Soc. Jpn.*, **51,** 2237 (1978).
30. a. J. P. Perchard, J. C. Monier, and P. Dizabo *Spectrochim. Acta Part A,* **27A,** 447 (1971). b. I. Kanesaka, R. G. Snyder, and H. L. Strauss, *J. Chem. Phys.*, **84,** 395 (1986).
31. a. Y.-C. Tse, M. D. Newton, and L. C. Allen, *Chem. Phys. Lett.*, **75,** 350 (1980). b. S. F. Smith, J. Chrandrasekhar, and W. L. Jorgensen, *J. Phys. Chem.*, **86,** 3308 (1982). c. R. L. Woodin and J. L. Beauchamp, *J. Am. Chem. Soc.*, **100,** 501 (1978).
32. R. M. Kennedy, M. Sagenkahn, and J. G. Aston, *J. Am. Chem. Soc.*, **63,** 2267 (1941).
33. F. Franks, M. A. J. Quickenden, D. S. Reid, and B. Watson, *Trans. Faraday Soc.*, **66,** 582 (1970).
34. O. Maass and E. H. Boomer, *J. Am. Chem. Soc.*, **44,** 1709 (1922).
35. K. A. Aronovich, L. P. Kastorskii, and K. F. Fedorova, *Zh. Fiz. Khim.*, **41,** 20 (1967).
36. W. L. Jorgensen, *Chem. Phys. Lett.*, **92,** 405 (1982).
37. J. L. Hales, H. A. Gundry, and J. H. Ellender, *J. Chem. Thermo.*, **15,** 211 (1983).
38. C. Carvajal, K. J. Tolle, J. Smid, and M. Szwarc, *J. Am. Chem. Soc.*, **87,** 5548 (1965).
39. I. A. Hossenlopp and D. W. Scott, *J. Chem. Thermo.*, **13,** 405 (1981).
40. D. V. S. Jain, R. K. Wadi, and S. B. Saini, *J. Chem. Thermo.*, **13,** 903 (1981).
41. L. G. Schornack and C. A. Eckert, *J. Phys. Chem.*, **74,** 3014 (1970).
42. a. W. L. Jorgensen and M. Ibrahim, *J. Am. Chem. Soc.*, **104,** 273 (1982). b. W. L. Jorgensen, *J. Am. Chem. Soc.*, **103,** 4721 (1981). c. W. L. Jorgensen and B. Bigot, *J. Phys. Chem.*, **86,** 2867 (1982).